ARTICLE

Chris Oostenbrink · Thereza A. Soares
Nico F. A. van der Vegt · Wilfred F. van Gunsteren

Validation of the 53A6 GROMOS force field

Abstract The quality of biomolecular dynamics simulations relies critically on the force field that is used to describe the interactions between particles in the system. Force fields, which are generally parameterized using experimental data on small molecules, can only prove themselves in realistic simulations of relevant biomolecular systems. In this work, we begin the validation of the new 53A6 GROMOS parameter set by examining three test cases. Simulations of the well-studied 129 residue protein hen egg-white lysozyme, of the DNA dodecamer d(CGCGAATTCGCG)$_2$, and a proteinogenic β^3-dodecapeptide were performed and analysed. It was found that the new parameter set performs as well as the previous parameter sets in terms of protein (45A3) and DNA (45A4) stability and that it is better at describing the folding–unfolding balance of the peptide. The latter is a property that is directly associated with the free enthalpy of hydration, to which the 53A6 parameter set was parameterized.

Keywords GROMOS · Force field · Molecular dynamics simulation · DNA · Lysozyme · β-Peptide

Introduction

Molecular dynamics simulations have become an established method in biomolecular chemistry to understand and predict important processes at the

C. Oostenbrink · T. A. Soares · W. F. van Gunsteren (✉)
Laboratory of Physical Chemistry, Swiss Federal
Institute of Technology, ETH-Hönggerberg,
8093 Zurich, Switzerland
E-mail: wfvgn@igc.phys.chem.ethz.ch
Tel.: +41-1-6325501
Fax: +41-1-6321039

N. F. A. van der Vegt
Computational Chemistry, Max-Planck-Institute
for Polymer Research, Ackermannweg 10,
55128 Mainz, Germany

molecular level. Numerically integrating the equations of motion for all relevant particles in a biomolecular system requires the availability of an accurate interaction function that describes the interaction between these particles, for instance through a classical force field. Several force fields exist for biomolecular simulation that are widely used, such as AMBER (Cornell et al. 1995; Pearlman et al. 1995; Weiner and Kollman 1981), CHARMM (Brooks et al. 1983; MacKerell et al. 1998; MacKerell et al. 1995), OPLS-AA (Jorgensen et al. 1996; Jorgensen and Tirado-Rives 1988) and GROMOS (Daura et al. 1998; Oostenbrink et al. 2004; Schuler et al. 2001; van Gunsteren and Berendsen 1987; van Gunsteren et al. 1996). Recently, it has been shown that all of these force fields severely underestimated the free energy of hydration for a series of small molecules that represent the amino acid side chains (MacCallum and Tieleman 2003; Shirts et al. 2003; Villa and Mark 2002). This was a very alarming finding, because for virtually all biomolecular processes of interest, the free energy of hydration and of transfer between polar and apolar media plays a vital role. Protein stability and folding, ligand recognition and binding, membrane formation and transport of small molecules across membranes are all being investigated by molecular dynamics simulations and all rely on a correct description of the equilibrium between 'solvation' of certain molecular moieties in different media.

Mainly for this reason, we have recently reparameterized many of the nonbonded interactions in the GROMOS force field specifically regarding the free enthalpy of hydration and of solvation in cyclohexane (Oostenbrink et al. 2004; Schuler et al. 2001). Unfortunately, it did not seem possible to obtain a parameter set for all polar functional groups that was at the same time able to accurately reproduce the density and heat of vaporization for pure liquids of small polar compounds. This was attributed to differences in average polarization of the molecules in different media. For this reason, we have proposed two new parameter sets: one that describes the interactions in pure liquids well and another

in which the free energies of hydration and solvation in cyclohexane for small functional groups (polar and apolar) are accurately reproduced. Together with several earlier parameter sets for lipids (Chandrasekhar et al. 2003), carbohydrates (Lins and Hünenberger 2005), nucleotides (Soares et al. 2005) and various (co)solvents (Fioroni et al. 2000; Geerke et al. 2004; Smith et al. 2004; Walser et al. 2000), this has led to the definition of the 53A5 (pure liquids) and 53A6 (hydration and solvation) parameter sets (Oostenbrink et al. 2004). The GROMOS force field is still a force field with a simple functional form (Scott et al. 1999; van Gunsteren et al. 1998) and a limited set of different atom types, bond types, bond-angle types, improper dihedral types and torsional-angle types. It makes use of the united atom approach for aliphatic hydrogens. These atoms are not treated explicitly, but are considered as a single interaction site together with the carbon atom to which they are bound.

However, no matter how much effort goes into parameterizing a force field, it can only prove its real worth in realistic biomolecular applications (van Gunsteren and Mark 1998). Previous GROMOS parameter sets [37C4 (Smith et al. 1995; van Gunsteren and Berendsen 1987), 43A1 (Daura et al. 1998; van Gunsteren et al. 1996) and 45A3 (Schuler et al. 2001; Schuler and van Gunsteren 2000)] have proven successful in describing biochemical interactions in protein stability (Antes et al. 2002; Bakowies and van Gunsteren 2002; Fan and Mark 2003, 2004; Smith et al. 1995, 1996, 1999; Stocker et al. 2000; Stocker and van Gunsteren 2000), peptide folding (Daura et al. 1999a; Daura et al. 2002; Daura et al. 1997; van Gunsteren et al. 2001) and protein-ligand binding (Hansson et al. 1998; Marelius et al. 1998; Oostenbrink et al. 2000; Oostenbrink and van Gunsteren 2004; Talhout et al. 2003). They have also been used successfully in simulations involving triglycerides (Chandrasekhar and van Gunsteren 2002), membranes (Chandrasekhar et al. 2003; Glättli et al., submitted) and DNA double helices (Bonvin et al. 1998; Czechtizky et al. 2001). For simulations of DNA double helices, a new parameter set has recently been introduced, with which it has proven to be possible to obtain stable simulations of DNA strands using a simple force field and cutoff scheme (Soares et al. 2005). In the current work, we want to begin validation of the 53A6 parameter set by simulating three relevant biomolecular systems or processes and comparing them to simulations that were performed with earlier parameter sets and to experimental data. In particular, because earlier parameter sets were parameterized on specific pair interactions (Hermans et al. 1984), and simulations were carried out on pure liquids of small molecules (Daura et al. 1998), it is interesting to see how a parameter set derived from free energies of hydration and solvation will perform.

As a first test case, we used hen egg-white lysozyme (HEWL), a well-studied, 129-residue protein for which ample experimental structural data from NMR experiments (Buck et al. 1995; Schwalbe et al. 2001; Smith et al. 1991, 1993) and X-ray crystallography (Artymiuk et al. 1982; Carter et al. 1997; Vaney et al. 1996) are available. It was also thoroughly studied by simulation earlier, allowing us to compare it with previous parameter sets (Smith et al. 1995; Soares et al. 2004; Stocker et al. 2000; Stocker and van Gunsteren 2000). It is of interest to investigate whether the 53A6 parameter set with new nonbonded parameters for all the neutral polar functional groups is still able to maintain the stability of the protein to the same extent.

For our second test case, we selected the DNA dodecamer d(CGCGAATTCGCG)$_2$, also known as the Dickerson–Drew dodecamer (Dickerson and Drew 1981; Drew and Dickerson 1981; Drew et al. 1981). This is another system for which both NMR data (Tjandra et al. 2000) and X-ray crystallographic structures (Dickerson and Drew 1981; Drew and Dickerson 1981; Drew et al. 1981; Shui et al. 1998) are available and which were studied previously with molecular dynamics techniques (Arthanari et al. 2003; Cheatham III and Kollman 2000; Cheatham III and Young 2000; Soares et al. 2005; Young et al. 1997). Only recently a new GROMOS parameter set, 45A4, has been introduced, with which it proved possible to obtain a stable simulation of this B-DNA double helix using a simple force field and cutoff scheme (Soares et al. 2005). Even though the charges on the nucleotide sugars and bases have not changed in the 53A6 parameter set, the van der Waals interaction for several atom types (C, O, N) have. It is therefore important to ensure that a simulation using the new parameter set does not deviate too much from the previous results.

As a third and final test case, we present a study on a β^3-dodecapeptide with proteinogenic side chains (a in Fig. 3). From NMR and CD experiments, this peptide is seen to form a 3_{14}-helix in methanol, while in water, no regular secondary structure elements could be observed (Etezady-Esfarjani et al. 2002). Simulations using the 45A3 parameter set starting from the experimental model structure rather showed the opposite. While the structure unfolded immediately in methanol, it seemed more stable in water. Since earlier peptide folding simulations using the same parameter set had shown good agreement with the experiment, this failure came as a surprise. It is most probably due to the relatively large number of polar side chains in the dodecapeptide compared to the ones simulated earlier (Daura et al. 1997, 1999a, 2002; Glättli et al. 2002a; Peter et al. 2000; van Gunsteren et al. 2001). In contrast to protein and DNA simulations, simulations of peptides cover timescales in which the folding–unfolding equilibrium is reached (Daura et al. 1997, 1999a, 2002; van Gunsteren et al. 2001); a process that will depend critically on the balance between hydrophilic and hydrophobic interactions. Since the parameter set 53A6 was parameterized specifically on this balance, one may expect major changes in a simulation of this peptide. Moreover, for about 60% of all atoms in this peptide, the charge and/or the van der Waals parameters have changed compared to

the 45A3/4 sets. The methanol model has slightly changed as well (Walser et al. 2000). Thus, in contrast to the HEWL and DNA simulations, one may expect the simulation characteristics of the β-peptide to change quite dramatically.

Methods

Simulations

Molecular dynamics simulations were performed using the GROMOS simulation package (Scott et al. 1999; van Gunsteren et al. 1996). Simulations on hen egg-white lysozyme (5 ns in water), the DNA dodecamer d(CGCGAATTCGCG)$_2$ (4 ns in water) and the β^3-dodecapeptide (100 ns in methanol; 25 ns in water) were carried out using the 53A6 parameter set.

The initial structure of the lysozyme was taken from the crystal structure (Artymiuk et al. 1982), protein data base (PDB) entry code 1AKI (Carter et al. 1997). The system was solvated in a periodically truncated octahedral box, containing 11,193 SPC (Berendsen et al. 1981) water molecules. The protonation states of protonatable groups were selected to correspond to a pH of 7. Eight chlorine ions were added to reach overall neutrality of the system, leading to a total of 34,910 atoms.

The simulations of the DNA dodecamer were also started from the crystal structure, PDB entry code 355D (Shui et al. 1998). The double helical structure was solvated in a rectangular periodic box containing 13,415 SPC water molecules, 46 sodium ions and 24 chlorine ions, corresponding to an overall neutral system with an ionic concentration of 0.1 M.

The β-dodecapeptide that was simulated is depicted in Fig. 3a. Simulations were started from the experimental model structure (Etezady-Esfarjani et al. 2002) in methanol solution (Fig. 3b). It was solvated in truncated octahedral boxes containing 5,506 SPC water molecules or 2,416 methanol molecules (Walser et al. 2000). No counter ions were added, yielding a net charge of $+4e$.

All simulations were carried out at a constant temperature of 298 K and a pressure of 1 atm using the weak coupling algorithm (Berendsen et al. 1984). Relaxation times were set to $\tau_T = 0.1$ ps and $\tau_P = 0.5$ ps and an estimated isothermal compressibility of 4.575×10^{-4} (kJ mol^{-1} nm^{-3})$^{-1}$ was used (van Gunsteren et al. 1996). All bond lengths were kept rigid at ideal bond lengths using the SHAKE algorithm (Ryckaert et al. 1977), allowing for a time step of 2 fs. Nonbonded interactions were calculated using a triple range cutoff scheme. Interactions within a short-range cutoff of 0.8 nm were calculated every time step from a pair list that was generated every five steps. At these time points, interactions between 0.8 and 1.4 nm were also calculated and kept constant between updates. A reaction-field contribution (Tironi et al. 1995) was added to the electrostatic interactions and forces to account for a homogeneous medium outside the long-range cutoff,

using a relative permittivity of 61 in the lysozyme and peptide simulations in water (Heinz et al. 2001), 66 in the DNA simulation (Glättli et al. 2002b) and 17.7 in the peptide simulation in methanol (Walser et al. 2000).

Analysis

All simulations described above were analysed together with very similar simulations that were performed earlier, using previous GROMOS parameter sets. The lysozyme simulations can be compared to a 3.5-ns simulation (Soares et al. 2004) based on the 45A3 parameter set (Schuler et al. 2001). For the DNA dodecamer, we also analysed a 4-ns trajectory from a simulation based on the 45A4 parameter set (Soares et al. 2005). Finally, the peptide simulations were compared to previous simulations based on the 45A3 parameter set (Schuler et al. 2001) and an older version of the methanol model (van Gunsteren et al. 1996).

Secondary structure assignments for the lysozyme simulations were carried out using the Kabsch and Sander rules (Kabsch and Sander 1983). Structural analyses of DNA base pair geometries were performed according to the rules as implemented in the 3DNA program (Lu and Olson 2003; Olson et al. 2001). Sugar-ring puckering was analysed through the pseudorotation phase and puckering amplitude as proposed by Altona and Sundaralingam (Altona et al. 1968; Altona and Sundaralingam 1972). Hydrogen bonds were analysed according to a geometrical criterion. A hydrogen bond is defined by a minimum donor-hydrogen-acceptor angle of 135° and a maximum hydrogen-acceptor distance of 0.25 nm (van Gunsteren et al. 1996).

Comparisons to NMR experimental data were made through an analysis of proton–proton distances as compared to NOE upper bounds. For lysozyme, a set of 1,630 NOE upper bounds was available (Schwalbe et al. 2001), for the DNA dodecamer, there were 160 upper bounds (Tjandra et al. 2000) and for the β-dodecapeptide we used 150 upper bounds, which were obtained in methanol (Etezady-Esfarjani et al. 2002). Proton–proton distances were averaged using $1/r^3$ averaging, $\bar{r} = \left(\langle r^{-3} \rangle \right)^{-1/3}$, corresponding to a slowly tumbling molecule (Tropp 1980). Positions of (aliphatic) protons that were not treated explicitly in the simulations were calculated from standard configurations. In cases where NOE upper bounds were assigned to more than one proton, a pseudoatom approach (Wüthrich et al. 1983) was used with the following corrections to the upper bound. For a non-stereospecifically assigned CHgroup, 0.09 nm was added to the upper bound. For a methyl group, the correction was 0.10 nm. For the six protons in an iso-propyl group, a correction of 0.22 nm was added and for unassigned H_δ and H_ϵ atoms in a flipping benzene ring, 0.21 nm. These corrections are very close to the pseudoatom corrections suggested by Wüthrich et al. (1983) and the ones used in the lysozyme structure determination (Schwalbe et al. 2001). They correspond

to the GROMOS standard bond lengths and angles (Oostenbrink et al. 2004; van Gunsteren et al. 1996). No additional multiplicity corrections (Constantine et al. 1992; Fletcher et al. 1996) were applied to the NOE upper bounds.

The simulations of the β-dodecapeptide were subjected to a conformational clustering analysis as described by Daura et al. (1999b). Snapshots of the simulations were taken at 0.01-ns intervals, and atom-positional root-mean-square differences (rmsd) between all pairs of structures were calculated using the backbone atoms (C, C_α, C_β, N) of residues 2 to 11. Structures with rmsd values smaller than 0.1 nm were considered to be structural neighbours. This tight criterion was chosen to distinguish small conformational differences. For every trajectory, the structure with the most neighbours was considered to be the central member of the (first, most populated) cluster of similar structures forming a conformation. After removing all structures belonging to this first cluster, the procedure was repeated to find the second, third etc. most populated clusters. Hydrogen bond analyses on all structures belonging to the ten most populated clusters have been carried out, using the criterion that was described above.

Results and discussion

Lysozyme

The overall structure of lysozyme is well maintained during a 5-ns simulation with the 53A6 parameter set. The atom-positional rmsd from the starting coordinates for the backbone atoms (N, C_α, C, O) gently increases during the first 2 ns of the simulation and levels off to an average value of 0.25 nm in the last 2 ns. In the 3.5-ns simulation using the 45A3 parameter set, it swiftly increased to 0.37 nm in the first 1.5 ns and remained stable at 0.39 nm over the course of the simulation (Soares et al. 2004).

A pictorial view of the stability can be found in Fig. 1, where the final structure after 5 ns (53A6) is fitted onto the original X-ray structure (Carter et al. 1997). Obviously, the fold is maintained and the most prominent secondary structure elements are preserved during the simulation. The conservation of the secondary structure elements is described in more detail in Table 1. Using the Kabsch and Sander (1983) assignment criteria, we averaged the secondary structure assignment of the residues over the secondary structure elements. Most elements that were seen in the X-ray structure (Carter et al. 1997) or in the bundle of NMR structures (Schwalbe et al. 2001) are also observed during the simulation. Of the four larger α-helices (indicated by A, B, C and D in Fig. 1 and Table 1), three are observed for about 90–100% of the time, while the fourth, helix D, seems to convert into a π-helix in our simulations. In particular, residues 111Trp to 115Cys appear to be in a π-helical arrangement for about 70% of the time in both

simulations. Interestingly, the D helix was observed only in 80% of the 50 NMR structures. In the other 20% of the NMR structures, a series of turns was assigned to these residues (Schwalbe et al. 2001). Similar conversions are seen for the helices 80Cys–84Leu and 120Val–124Ile. In the crystal structure, these are assigned 3_{10}-helices, but in the NMR structures and our simulations, the α-helix seems to be preferred. The other two 3_{10}-helices in the X-ray structure also seem to be represented poorly in the course of the simulations (20Tyr–22Gly and 104Gly–107Ala). On the other hand, a β-bridge is present for 83% of the time between residues 19Asn and 23Tyr in the 53A6 simulation. Also, the hydrogen bond 23Tyr to 20Tyr is observed for 71% in our hydrogen bond analysis. Similarly, for the helix 104Gly – 107Ala, several turns can be observed and hydrogen bonds for 106Asn to 104Gly and 108Trp to 105Met are observed for about 20% of the time each. The anti-parallel β-sheet involving residues in the range of 43Thr to 59Asn is maintained for well over 90% of the time, as are the β-bridges 2Val–39Asn and 65Asn–79Pro.

A summary of the NOE analysis that was performed on both simulations can be found in Table 2. A total of 1,630 NOE upper bounds were taken into account in the
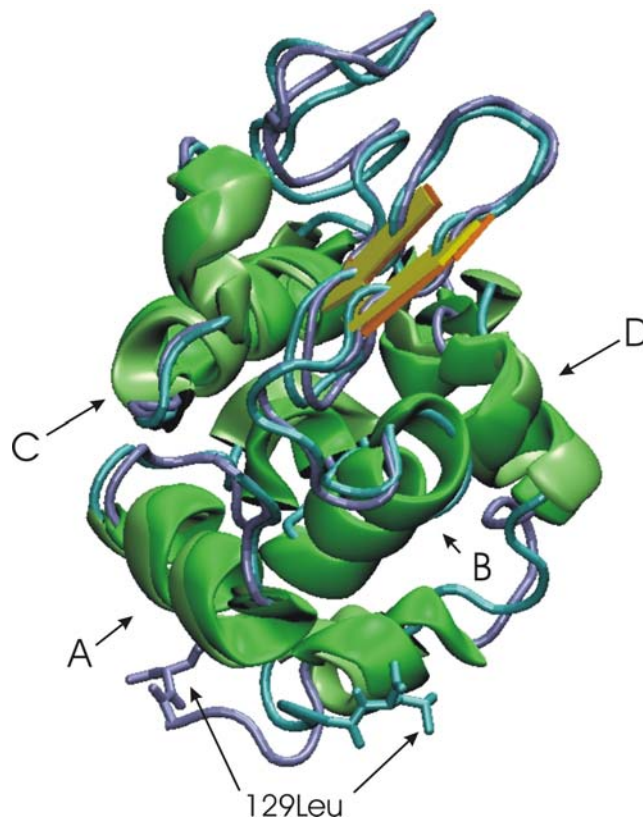

Fig. 1 Overlay of the hen egg-white lysozyme crystal structure and the structure obtained after 5 ns of simulation. Crystal structure in *dark blue* (backbone), *green* (helices) and *orange* (sheets). Simulation structure in *light blue* (backbone), *light green* (helices) and *yellow* (sheets). Large α-helices *A*, *B*, *C*, and *D* (see Table 1) are indicated, as well as the position of the C-terminal 129Leu

Table 1 Secondary structure analysis of lysozyme

Residues	Number of residues	Secondary structure	Average occurrence 45A3 (%)	Average occurrence 53A6 (%)
2Val–39Asn	2	β-Bridge[a,b]	96	99
5Arg–14Arg (A)	10	α-Helix[a,b]	99	100
20Tyr–22Gly	3	3_{10}-Helix[a]	5	12
19Asn–23Tyr	2	β-Bridge	10	84
25Leu–36Ser (B)	11	α-Helix[a,b]	78	94
		π-Helix	2	5
		3_{10}-Helix	4	0
43Thr–45Arg	3	β-Sheet[a,b]	97	91
51Thr–53Tyr	3	β-Sheet[a,b]	99	98
58Ile–59Asn	2	β-Sheet[a]	98	99
60Ser–63Trp	4	α-Helix	25	4
65Asn–79Pro	2	β-Bridge[a]	71	92
80Cys–84Leu	5	3_{10}-Helix[a,b]	26	25
		α-Helix[b]	55	52
89Thr–101Asp (C)	13	α-Helix[a,b]	89	89
		π-Helix	1	4
104Gly–107Ala	4	3_{10}-Helix[a]	9	3
		α-Helix	0	0
109Val–114Arg (D)	6	α-Helix[a,b]	37	11
		π-Helix	50	61
120Val–124Ile	5	3_{10}-Helix[a]	23	20
		α-Helix[b]	35	41

For every secondary structure element the secondary structure assignment according to Kabsch and Sander (1983) was averaged over time (3.5 ns for 45A3; 5.0 ns for 53A6) and number of residues involved (second column)
[a]Observed in crystal structure (Carter et al. 1997)
[b]Observed in NMR structures (Schwalbe et al. 2001)

analysis (Schwalbe et al. 2001). In line with the development of the rmsd, one sees an increase in the total number of violations during the first 1.5 ns of the simulations and a more converged number of violations in the latter part of the simulations. Both simulations satisfy about 95% of the experimental upper bounds within 0.1 nm. Of the 13 large violations (>0.3 nm) that were observed in the 1.5 to 3.5-ns part of the 53A6 simulation, six involved the C-terminal 129Leu. As indicated in Fig. 1, the C-terminus turns around in the course of the 53A6 simulation. Removing the 22 NOE upper bounds involving 129Leu from the experimental set significantly reduces the number of violations and the average vio-

lation for the 53A6 simulation, but not for the 45A3 simulation. The termini of a protein are known to be much more flexible and a movement as depicted in Fig. 1 is not likely to affect the overall stability of the protein. However, it can be expected that a 5-ns simulation is not sufficient to sample all C-terminal motions, such that the NOE upper bounds for this region would be reproduced.

DNA dodecamer

Both of the tested parameter sets maintain an overall double helical structure of the DNA dodecamer. Rmsd deviations from the initial crystal structure for all heavy atoms fluctuate around 0.4–0.5 nm in the last 2 ns of the simulation. As a general trend, it was observed that the backbone atoms show larger rmsd values than the atoms in the bases. Fluctuations in the atomic positions are strongest in the first and last base pairs. This can also be seen from an investigation of the Watson–Crick hydrogen bonds as displayed in Fig. 2. Hydrogen bonds in the middle base pairs are well maintained during the course of the simulation, while the first and the last base pairs are less strongly bound. In the 53A6 simulation, the last base pair opens up completely, slightly earlier than in the 45A4 simulation, resulting in a lower number of hydrogen bonds. It is known that the first and last base pairs show considerable mobility and we note that none of the NMR model structures satisfies all experimental data involving these bases (Tjandra et al. 2000).

Structural parameters for the bases and sugar puckering are presented in Table 3. All properties are averaged over the 12 base pairs. It should be noted explicitly that the data presented for the parameter sets 45A4 and 53A6 are averages over 10,000 structures from the 4-ns simulations, whereas the NMR and X-ray data are averaged over five structures (Tjandra et al. 2000) and a single structure (Shui et al. 1998), respectively. This becomes especially apparent from the distribution of the sugar pucker, where in the NMR structures only C1'-exo and C2'-endo conformations were seen. Tjandra et al. (2000) noted that this does not mean that the sugar

Table 2 Number of NOE upper-distance-bound violations and average violations in the lysozyme simulations for different averaging periods

Averaging time period (ns)	Force-field parameter set	NOE upper-bound violations >0.1 nm	NOE upper-bound violations >0.2 nm	NOE upper-bound violations >0.3 nm	Average violation (nm)
0.5–1.5	45A3	61 (4%)	22 (1%)	6 (0.4%)	0.011
	53A6	68 (4%)	27 (1%)	7 (0.4%)	0.012
1.5–3.5	45A3	73 (4%)	34 (2%)	14 (0.9%)	0.013
	45A3 no 129	72 (4%)	34 (2%)	14 (0.9%)	0.013
	53A6	86 (5%)	37 (2%)	13 (0.8%)	0.017
	53A6 no 129	78 (5%)	31 (2%)	7 (0.4%)	0.014
3.5–5.0	53A6	86 (5%)	41 (3%)	14 (0.9%)	0.018

The percentage of the total number of NOE upper bounds is given in brackets. no129 indicates the analysis where all (22) upper bounds involving residue 129Leu have been left out
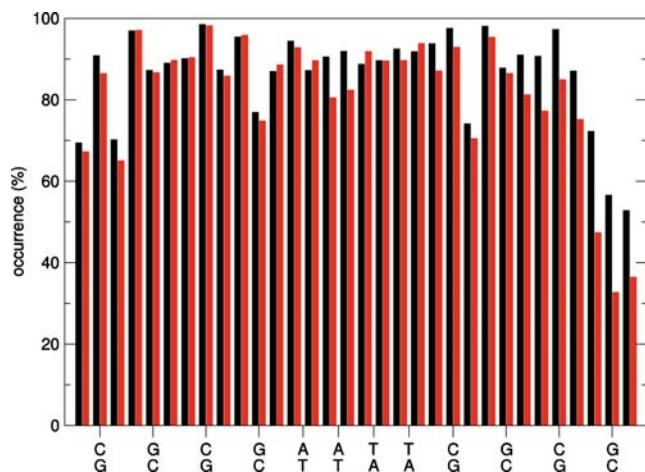
Fig. 2 Occurrence of the Watson-Crick hydrogen bonds in 4-ns DNA simulations using the 45A4 (*black*) and 53A6 (*red*) parameter sets. For every base pair, three or two hydrogen bonds are given

puckering is in reality not more dynamic. The pucker distribution from the simulations as given in Table 3 is observed for all individual sugar rings, with the exception of the sugar ring of Ade (6) which shows a C3′-endo puckering for 13% (45A4) and 18% (53A6) in the simulations.

The averages over some of the structural properties (X-displacement, helical rise, inclination, helical twist, slide, roll and twist) show significant deviations from the values for canonical B-DNA and indicate that the dodecamer moves towards the A-DNA form (Olson et al. 2001). A downward trend can also be observed in the rmsd with respect to a canonical A-DNA structure during the course of the simulation (data not shown). Apparently, the dodecamer covers a part of conformational space that lies between the canonical A-DNA and B-DNA forms. Whether this is an artefact of the simulation or a true representation of the dynamic structure of this dodecamer in solution remains open.

Table 4 summarizes the NOE distance analyses for the simulation trajectories, for the NMR model structures (Tjandra et al. 2000), the X-ray (B-DNA) structure (Shui et al. 1998), and for a modelled canonical A-DNA structure with the same sequence. Proton–proton distances were averaged over the simulation period from 1 to 4 ns. Different averaging times showed very similar results. As in the lysozyme test case, about 95% of the 160 experimental upper bounds were satisfied within 0.1 nm. The 53A6 simulation shows slightly more violations larger than 0.1 nm, with a maximum violation of 0.128 nm between H1′ of Ade (6) and and H5′ of Thy (7) in the second chain. The largest violation in the 45A4 simulation amounts to 0.295 nm between H1′ of Thy (8) and H5′ of Cyt (9) of the first chain. In both simulations, only 1 of the 20 NOE upper bounds that involve the first and last base pairs shows a violation larger than 0.1 nm, indicating that the large flexibility that is observed in the simulations is not in contrast with the experimental NMR data.

Table 3 Comparison of structural parameters obtained from experimental and simulation structures of the DNA dodecamer

	45A4	53A6	NMR	X-ray
Local base-pair parameters				
Shear (nm)	−0.002	0.007	0.0	−0.018
Stretch (nm)	−0.017	−0.017	−0.039	−0.015
Stagger (nm)	−0.035	−0.033	−0.022	−0.002
Buckle (°)	0.0	−0.6	−0.1	2.5
Propeller (°)	−7.1	−7.1	−12.3	−19.0
Opening (°)	−2.0	−2.2	2.1	3.0
Sugar-ring puckering				
C3′-endo (%)	5	4	0	4
C4′-exo (%)	4	4	0	0
O4′-endo (%)	20	19	0	12
C1′-exo (%)	44	44	63	42
C2′-endo (%)	23	25	37	42
C3′-exo (%)	2	2	0	0
C2′-exo (%)	1	1	0	0
Pseudorotation				
Phase (°)	118.8	121.1	132.1	133.7
Amplitude (°)	42.5	42.4	29.3	41.3
Local base-pair helical parameters				
X-displacement (nm)	−0.349	−0.321	−0.128	−0.052
Y-displacement (nm)	0.004	−0.009	0.001	−0.022
Rise (nm)	0.278	0.300	0.329	0.329
Inclination (°)	15.5	14.2	4.6	5.0
Tip (°)	−0.2	−0.1	0.0	1.3
Helical twist (°)	33.4	33.3	35.1	37.8
Local base-pair step parameters				
Shift (nm)	−0.002	0.003	0.0	0.002
Slide (nm)	−0.109	−0.092	−0.046	0.004
Rise (nm)	0.342	0.357	0.338	0.341
Tilt (°)	0.1	0.1	0.0	−0.9
Roll (°)	8.4	7.8	2.5	3.4
Twist (°)	30.4	30.5	34.6	36.1

Averages are over all bases, sugars, base pairs and inter-base-pair parameters observed in 4 ns of simulation (parameter sets 45A3 and 53A6), five NMR model structures (Tjandra et al. 2000) or the X-ray structure (Shui et al. 1998). Local base-pair parameters, helical parameters and step parameters were calculated using the three DNA definitions (Lu and Olson 2003; Olson et al. 2001). Sugar puckering, pseudorotation phase and pucker amplitudes are according to Altona et al. (1968) and Altona and Sundaralingam (1972)

Table 4 Number of NOE upper-bound violations and average violations in the DNA dodecamer simulations

Force-field parameter set	NOE upper-bound violations			Average violation (nm)
	> 0.05 nm	> 0.1 nm	> 0.2 nm	
45A3	45 (28%)	3 (2%)	1 (0,6%)	0.029
53A6	50 (31%)	8 (5%)	0	0.032
NMR[a]	6 (4%)	0	0	0.012
B-DNA[b]	52 (33%)	23 (14%)	2 (1%)	0.042
A-DNA[c]	72 (45%)	38 (24%)	0	0.058

The percentage of the total number of NOE upper bounds is given in brackets. For the simulations, averaging was performed over the last 3 ns of simulation
[a] Average over five NMR structures (Tjandra et al. 2000)
[b] Single X-ray structure (Shui et al. 1998)
[c] Modelled canonical A-DNA structure

Table 4 also includes the NOE violations for the NMR bundle of model structures as well as for the X-ray structure (labelled B-DNA) and a modelled A-DNA structure. As could be expected, the NMR structures that were derived based on the NOE upper bounds show very small violations. NOE analyses of single structures (X-ray and A-DNA model structures), however, show many violations, indicating that the averaging effect of a dynamic simulation is required to reproduce the NOE upper bounds. Of the 38 violations larger than 0.1 nm in the A-DNA model, only 1 also shows a large deviation in the simulations. For the 45A4 simulation, this is (again) the NOE between H1′ of Thy (8) and H5′ of Cyt (9) of the first chain (at 0.295 nm), and for the 53A6 simulation it is the NOE between H1′ in Gua (10) and H6 in Cyt (11) in the second chain (at 0.111 nm). Even though the structural parameters that were described above might indicate a drift towards an A-DNA conformation, the simulations are not in contrast with the NMR data and do not show the violations of the upper bounds that one might expect from a pure A-DNA conformation.

β^3-Dodecapeptide

The simulations of the β-dodecamer were all started from the folded helical experimental model structure (Etezady-Esfarjani et al. 2002). For a peptide of this length, the time required for the complete folding process from a random or extended conformation can still be expected to be beyond the length of these simulations. For the four simulations, a clustering analysis was performed (Daura et al. 1999b) with a similarity criterion of 0.1 nm as described in Methods. For a peptide of this length with 40 atoms that are taken into account in the fitting and rmsd calculation, 0.1 nm is a relatively small value. This means that once the peptide samples a broad ensemble of structures in conformational space, one might expect very many different clusters, whereas a low number of clusters means that the conformation of the peptide does not change much. Table 5 lists the total number of clusters that was found in every simulation. It is clear that the 45A3 simulation of the peptide in methanol samples many more conformations than the other simulations. Taking the shortest simulation time of 25 ns into account, the 53A6 simulation in water could well be sampling the second highest number of conformations. Table 5 also lists the average number of 3_{14}-helical hydrogen bonds for the ten most populated clusters and for all simulation structures. The average is taken over the theoretically 10 3_{14}-helical hydrogen bonds that could be formed in this peptide. The number of hydrogen bonds that is actually observed in the cluster is given in brackets.

In Fig. 3c–f, we depict the central member structure of the most populated cluster from each of the four simulations (45A3 in methanol, 53A6 in methanol, 45A3 in water and 53A6 in water). It is obvious that the most populated cluster of the simulation in methanol using the 45A3 parameter set does not represent a helical conformation, whereas the others do. Table 5 shows that the most populated cluster in the 45A3 simulation in methanol only represents 7.8% of the total simulation time. Other clusters with an even lower occupancy do show some helical content as can be seen from the hydrogen bond analyses. These clusters only contain structures from the first 30 ns of the simulation. Overall,

Table 5 Summary of conformational clustering results for the entire simulations of the β-dodecapeptide

Force field	45A3				53A6			
Solvent	MeOH		H$_2$O		MeOH		H$_2$O	
Simulation length (ns)	100		100		100		25	
Number of clusters	1868		410		239		240	
	Percentage	Hydrogen bonds	Percentage	Hydrogen bonds	Percentage	Hydrogen bonds	Percentage	Hydrogen bonds
Cluster 1	7.8	0	34.0	52 (9)	59.5	73 (10)	20.9	61 (10)
Cluster 2	2.5	59 (8)	6.6	0	4.5	57 (8)	3.7	7 (10)
Cluster 3	1.4	35 (8)	4.2	60 (10)	3.6	46 (6)	3.2	0
Cluster 4	1.3	0	3.0	0	1.7	49 (6)	2.7	10 (3)
Cluster 5	1.2	38 (7)	2.5	0	1.5	49 (6)	1.7	9 (2)
Cluster 6	1.2	44 (7)	2.3	0	1.1	73 (10)	1.5	28 (5)
Cluster 7	1.1	44 (5)	2.1	0	1.1	61 (7)	1.5	1 (1)
Cluster 8	0.8	35 (5)	1.9	18 (2)	1.0	42 (6)	1.4	1 (1)
Cluster 9	0.8	0	1.4	22 (4)	1.0	29 (3)	1.3	69 (10)
Cluster 10	0.7	41 (7)	1.4	42 (8)	0.9	29 (3)	1.2	1 (1)
Overall	100	12 (10)	100	29 (10)	100	60 (10)	100	20 (10)

Clustering criterion: a backbone atom-positional root-mean-square deviation smaller than 0.1 nm. For the ten most populated conformations observed in simulations using the 45A3 and 53A6 parameter sets in methanol (MeOH) and water (H$_2$O), the occurrence is given (columns labelled with 'percentage') as well as the average occurrence of the 10 3_{14}-helical hydrogen bonds in that cluster (columns labelled with 'hydrogen bonds'). The total number of helical hydrogen bonds observed are given in brackets
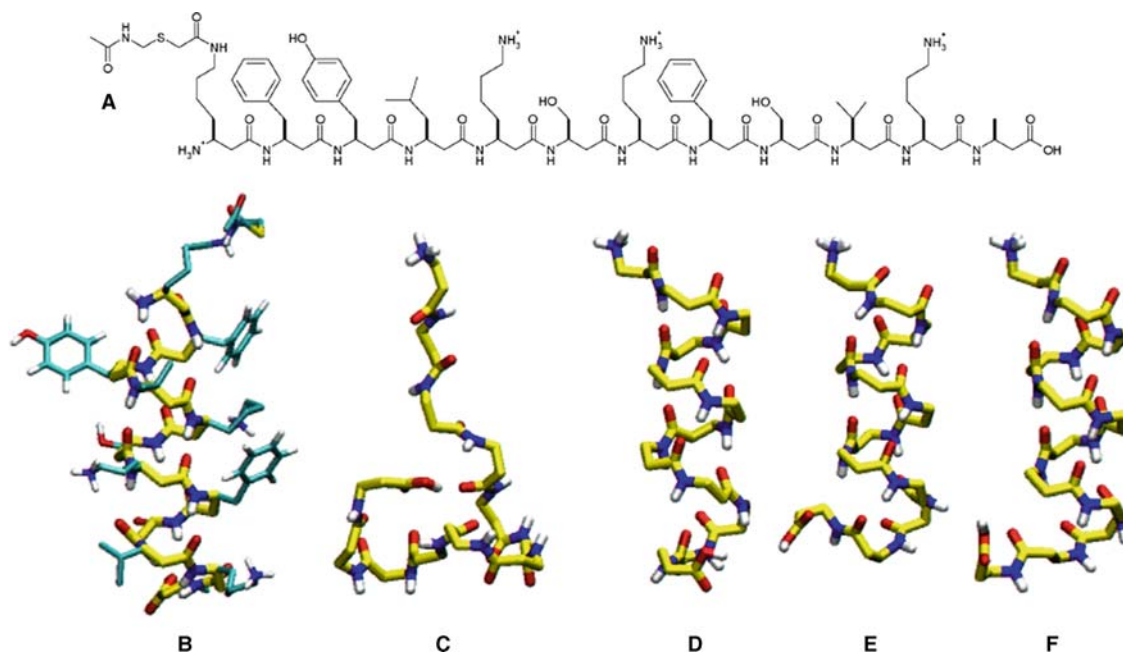
Fig. 3 Chemical formula of the dodecapeptide (**a**). Stick representation of the experimental NMR model structure with backbone carbon atoms in *yellow*, sidechains in *blue* (**b**). Stick representation of the backbone of the central member structures of the most populated conformational clusters using parameter set 45A3 in methanol (**c**), 53A6 in methanol (**d**), 45A3 in water (**e**) and 53A6 in water (**f**)

the 3_{14}-helical hydrogen bonds are seen only for 12% of the time in the simulation using the 45A3 parameter set. Figure 4 shows the rmsd for the backbone atoms (N, C_α, C_β, C) with respect to the experimental NMR model structure. It is clear that this simulation strongly deviates from the NMR model structure for most of the 100 ns. The experimental structure is revisited to within an rmsd

Fig. 4 Atom-positional root-mean-square-deviations of the backbone atoms (C, C_α, C_β, N) of residues 2–11 with respect to the experimental NMR model structure derived for the peptide in methanol. Parameter sets 45A3 (*black*) and 53A6 (*red*) in methanol (**a**) and water (**b**)

value of 0.04 nm after approximately 24 ns, but is quickly abandoned again. This indicates that the absence of significant helical conformations is not due to insufficient sampling, but rather to a low energetic stability of this conformation.

For the simulation in methanol using the 53A6 parameter set, we see quite the opposite picture. The low number of clusters indicates that the peptide is very stable throughout the simulation, as can also be observed in Fig. 4. The hydrogen bond analysis (Table 5) shows that the cluster that represents 60% of the simulation shows 73% of the helical hydrogen bonds, and that all subsequent clusters displayed here show a significant helical content. The overall presence of 3_{14}-helical hydrogen bonds is with 60% the highest of the four simulations. From Fig. 4, we see that the peptide does deviate from the experimental structure for some periods in the simulation, but also finds its way back again to the original conformation after 22 and 75 ns.

In water, where no evidence of regular secondary structure was found experimentally, the 45A3 simulation seems to find a stable conformation (cluster 1, see Fig. 3e) close to the NMR model structure up to about 38 ns, after which it unfolds, and revisits the same conformation again at 50 and 55 ns. After this point in time, the helical structure is lost and clusters 2, 4, 5, 6 and 7 in Table 5 come into play. Overall, the 3_{14}-helical hydrogen bonds are observed for about 29%, much more than in the methanol simulation with the same parameter set. The 53A6 simulation in water, even though much shorter, seems to be stable in clusters 1 and 9 for about 7.5 ns, after which the peptide visits cluster 6, which is still about half helical. The other clusters that are visited seem to be far away from the NMR model structure, with the occasional appearance of helical hydrogen bonds.
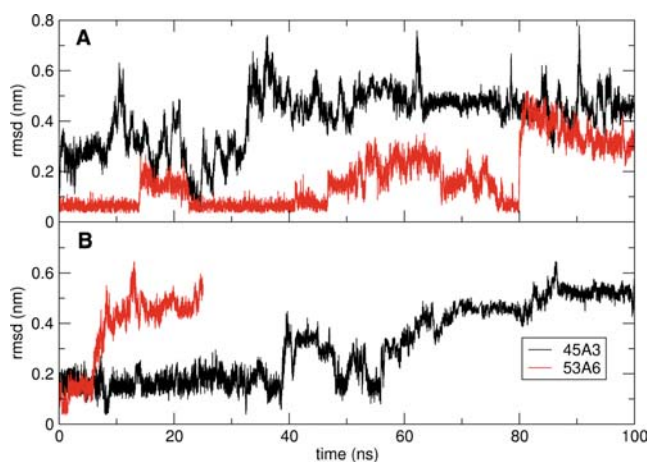
Table 6 Number of NOE upper bound violations and average (over the entire simulations) violations in the β^3-dodecapeptide simulations

Force-field parameter set	Solvent	NOE upper bound violations			Average violation (nm)
		> 0.05 nm	> 0.1 nm	> 0.2 nm	
45A3	MeOH	34 (23%)	25 (17%)	13 (9%)	0.043
	H_2O	26 (17%)	11 (7%)	3 (2%)	0.023
53A6	MeOH	12 (8%)	3 (2%)	0	0.010
	H_2O	33 (22%)	21 (14%)	5 (3%)	0.030

The percentage of the total number of NOE upper bounds is given in brackets. The NOE upper bounds have been derived from NMR experiments on the β-dodecapeptide in methanol. No NOE bounds for the peptide in water were available

In summary, we can conclude that the simulations with the 45A3 parameter sets do not seem to reproduce the experimental finding of a 3_{14}-helix in methanol and no regular secondary structure in water. In the 45A3 simulations in methanol the 3_{14}-helix is not stable, whereas in water it seems to be more stable, but also unfolding. Using the parameter set 53A6, the simulations do agree with the experiment; in methanol, the 3_{14}-helical structure seems stable, the peptide goes away from this structure and refolds to it later on. In water, the 3_{14}-helical structure seems much less stable, unfolding after about 7.5 ns. The NOE analyses on these simulations nicely mirror these findings. As can be seen from Table 6, the 45A3 parameter set in methanol performs worst in reproducing the experimental upper bounds. Even though the experimental data was obtained in methanol, the simulations in water seem to agree better. The best agreement with the experiment is obtained from the simulation using the 53A6 parameter set in methanol, which shows a very low number of violations and a very low average violation. The 53A6 parameter set, which was parameterized specifically on the free enthalpies of hydration and of solvation in cyclohexane, seems more able to reproduce the experimental data in a folding study of a peptide containing polar groups. Of course, the balance between different 'solvation' states of the different groups in the peptide will be directly associated to the folding stability and equilibrium.

Conclusion

We have presented three test cases in order to begin the validation of the new GROMOS 53A6 parameter set (Oostenbrink et al. 2004) for biomolecular simulation. The simulation of the 129-residue protein hen egg-white lysozyme remains stable over 5 ns. Secondary structure elements are well preserved and 95% of the proton–proton upper bounds derived from NMR experiments is reproduced within 0.1 nm. The same goes for the simulation of the DNA dodecamer, which was stable for 4 ns. Fluctuations at the end of the chains were not in contrast with the NMR data that were used. Structural parameters indicate that the dodecamer visits conformations that are between the canonical A-DNA and B-DNA forms, which is also not in contrast with the NMR data. No major differences between simulations with previous parameter sets and the new parameters were observed in these two test cases.

For the β^3-dodecapeptide, significant differences between the two parameter sets were observed. In a long simulation in which a folding–unfolding equilibrium can be established, the balance between different 'solvation' states of the different functional groups will be of vital importance. We showed that simulations with a parameter set that was derived from the free enthalpies of hydration and of apolar solvation reproduce the experimentally found secondary structure better than the previous parameter set.

Overall, the 53A6 parameter set behaves similarly to the previous (45A3/4) GROMOS parameter sets in terms of protein and DNA stability. In a case where the balance between different environments of polar groups plays an important role, it performed better in reproducing the experimental data. After these initial validations, we think it is safe to use this parameter set in the future and are confident that it will prove itself in many simulations to come.

References

Altona C, Sundaralingam M (1972) Conformational analysis of the sugar ring in nucleosides and nucleotides. A new description using the concept of pseudorotation. J Am Chem Soc 94:8205–8212

Altona C, Geise HJ, Romers C (1968) Conformation of non-aromatic ring compounds-XXV. Geometry and conformation of ring D in some steroids from X-ray structure determinations. Tetrahedron 24:13–32

Antes I, Thiel W, Gunsteren WF van (2002) Molecular dynamics simulations of photoactive yellow protein (PYP) in three states of its photocycle: a comparison with X-ray and NMR data and analysis of the effects of Glu46 deprotonation and mutation. Eur Biophys J 31:504–520

Arthanari H, McConnell KJ, Beger R, Young MA, Beveridge DL, Bolton PH (2003) Assessment of the molecular dynamics structure of DNA in solution based on calculated and observed NMR NOESY volumes and dihedral angles from scalar coupling constants. Biopolymers 68:3–15

Artymiuk PJ, Blake CCF, Rice DW, Wilson KS (1982) The structures of the monoclinic and orthorhombic forms of hen egg-white lysozyme at 6 Å resolution. Acta Cryst B38:778–783

Bakowies D, Gunsteren WF van (2002) Simulations of apo- and holo-fatty acid binding protein: structure and dynamics of protein, ligand and internal water. J Mol Biol 315:713–736

Berendsen HJC, Postma JPM, Gunsteren WF van, Hermans J (1981) Interaction models for water in relation to protein hydration. In: Pullman B (ed) Intermolecular forces. Reidel, Dordrecht, pp 331–342

Berendsen HJC, Postma JPM, Gunsteren WF van, DiNola A, Haak JR (1984) Molecular-dynamics with coupling to an external bath. J Chem Phys 81:3684–3690

Bonvin AMJJ, Sunnerhagen M, Otting G, Gunsteren WF van (1998) Water molecules in DNA recognition II: a molecular dynamics view of the structure and hydration of the Trp operator. J Mol Biol 282:859–873

Brooks BR, Bruccoleri RE, Olafson BD, States DJ, Swaminathan S, Karplus M (1983) CHARMM - A program for macromolecular energy, minimization and dynamics calculations. J Comput Chem 4:187–217

Buck M, Boyd DB, Redfield C, MacKenzie DA, Jeenes DJ, Archer DB, Dobson CM (1995) Structural determinants of protein dynamics: analysis of ^{15}N NMR relaxation measurements for main-chain and side-chain nuclei of hen egg white lysozyme. Biochemistry 34:4041–4055

Carter D, He J, Ruble JR, Wright B (1997) The structure of the orthorhombic form of hen egg-white lysozyme at 1.5 Å resolution. Protein Data Bank, entry 1AKI

Chandrasekhar I, Gunsteren WF van (2002) A comparison of the potential energy parameters of aliphatic alkanes: molecular dynamics simulations of triacylglycerols in the alpha phase. Eur Biophys J 31:89–101

Chandrasekhar I, Kastenholz MA, Lins RD, Oostenbrink C, Schuler LD, Tieleman DP, Gunsteren WF van (2003) A consistent potential energy parameter set for lipids: dipalmitoylphosphatidylcholine as a benchmark of the GROMOS96 45A3 force field. Eur Biophys J 32:67–77

Cheatham III TE, Kollman PA (2000) Molecular dynamics simulation of nucleic acids. Annu Rev Phys Chem 51:435–471

Cheatham III TE, Young MA (2000) Molecular dynamics simulation of nucleic acids: successes, limitations, and promise. Biopolymers 56:232–256

Constantine KL, Madrid M, Bányai L, Trexler M, Patthy L, Llinás M (1992) Refined solution structure and ligand-binding properties of PDC-109 domain b. A collagen-binding type II domain. J Mol Biol 223:281–298

Cornell WD, Cieplak P, Bayly CI, Gould IR, Mertz KM, Ferguson DM, Spellmeyer DC, Fox T, Caldwell JW, Kollman PA (1995) A second generation force field for the simulation of proteins, nucleic acids and organic molecules. J Am Chem Soc 117:5179–5197

Czechtizky W, Daura X, Vasella A, Gunsteren WF van (2001) Oligonucleotide analogues with a nucleobase-including backbone. Part 7: molecular dynamics simulation of a DNA duplex containing a 2′-deoxyadenosine 8-(hydroxymethyl)-derived nucleotide. Helv Chim Acta 84:2132–2145

Daura X, Gunsteren WF van, Rigo D, Jaun B, Seebach D (1997) Studying the stability of a helical ß-heptapeptide by molecular dynamics simulations. Chem Eur J 3:1410–1417

Daura X, Mark AE, Gunsteren WF van (1998) Parametrization of aliphatic CHn united atoms of GROMOS96 force field. J Comput Chem 19:535–547

Daura X, Gademann K, Jaun B, Seebach D, Gunsteren WF van, Mark AE (1999a) Peptide folding: when simulation meets experiment. Angew Chem Int Ed 38:236–240

Daura X, Gunsteren WF van, Mark AE (1999b) Folding-unfolding thermodynamics of a β-heptapeptide from equilibrium simulations. Proteins 34:269–280

Daura X, Glättli A, Gee P, Peter C, Gunsteren WF van (2002) The unfolded state of peptides. Adv Protein Chem 62:341–360

Dickerson RE, Drew HR (1981) Structure of a B-DNA dodecamer. 2. Influence of base sequence on helix structure. J Mol Biol 149:761–786

Drew HR, Dickerson RE (1981) Structure of a B-DNA dodecamer. 3. Geometry of hydration. J Mol Biol 151:535–556

Drew HR, Wing RM, Takano T, Broka C, Tanaka S, Itakura K, Dickerson RE (1981) Structure of a B-DNA dodecamer—conformation and dynamics. Proc Natl Acad Sci USA 78:2179–2183

Etezady-Esfarjani T, Hilty C, Wüthrich K, Rueping M, Schreiber J, Seebach D (2002) NMR-structural investigations of a β^3-dodecapeptide with proteinogenic side chains in methanol and in aqueous solutions. Helv Chim Acta 85:1197–1209

Fan H, Mark AE (2003) Relative stability of protein structures determined by X-ray crystallography or NMR spectroscopy: a molecular dynamics simulation study. Proteins 53:111–120

Fan H, Mark AE (2004) Refinement of homology-based protein structures by molecular dynamics simulation techniques. Protein Sci 13:211–220

Fioroni M, Burger K, Mark AE, Roccatano D (2000) A new 2,2,2-trifluoroethanol model for molecular dynamics simulations. J Phys Chem B 104:12347–12354

Fletcher CM, Jones DNM, Diamond R, Neuhaus D (1996) Treatment of NOE constraints involving equivalent or nonstereoassigned protons in calculations of biomacromolecular structures. J Biomol NMR 8:292–310

Geerke DP, Oostenbrink C, Vegt NFA van der, Gunsteren WF van (2004) An effective force field for molecular dynamics simulations of dimethyl sulfoxide and dimethyl sulfoxide-water mixtures. J Phys Chem B 108:1436–1445

Glättli A, Daura X, Seebach D, Gunsteren WF van (2002a) Can one derive the conformational preference of a beta-peptide from its CD spectrum. J Am Chem Soc 124:12972–12184

Glättli A, Daura X, Gunsteren WF van (2002b) Derivation of an improved simple point charge model for liquid water: SPC/A and SPC/L. J Chem Phys 116:9811–9828

Gunsteren WF van, Berendsen HJC (1987) Groningen molecular simulation (GROMOS) library manual. Biomos, Groningen

Gunsteren WF van, Mark AE (1998) Validation of molecular dynamics simulation. J Chem Phys 108:6109–6116

Gunsteren WF van, Billeter SR, Eising AA, Hünenberger PH, Krüger P, Mark AE, Scott WRP, Tironi IG (1996) Biomolecular simulation: the GROMOS96 manual and user guide. Vdf Hochschulverlag AG an der ETH Zürich, Zürich

Gunsteren WF van, Daura X, Mark AE (1998) GROMOS force field. In: von Ragué Schleyer P (ed) Encyclopedia of computational chemistry, vol 2. Wiley, New York, pp 1211–1216

Gunsteren WF van, Bürgi R, Peter C, Daura X (2001) The key to solving the protein-folding problem lies in an accurate description of the denatured state. Angew Chem Int Ed 40:351–355

Hansson T, Marelius J, Åqvist J (1998) Ligand binding affinity prediction by linear interaction energy methods. J Comput-Aid Mol Des 12:27–35

Heinz TN, Gunsteren WF van, Hünenberger PH (2001) Comparison of four methods to compute the dielectric permittivity of liquids from molecular dynamics simulations. J Chem Phys 115:1125–1136

Hermans J, Berendsen HJC, Gunsteren WF van, Postma JPM (1984) A consistent empirical potential for water-protein interactions. Biopolymers 23:1513–1518

Jorgensen WL, Tirado-Rives J (1988) The OPLS potential functions for proteins—energy minimizations for crystals of cyclic peptides and crambin. J Am Chem Soc 110:1657–1666

Jorgensen WL, Maxwell DS, Tirado-Rives J (1996) Development and testing of the OPLS all-atom force field on conformational energetics and properties of organic liquids. J Am Chem Soc 118:11225–11236

Kabsch W, Sander C (1983) Dictionary of protein secondary structure: pattern recognition of hydrogen-bonded and geometrical features. Biopolymers 22:2577–2637

Lins RD, Hünenberger PH (2005) A new GROMOS parameter set for hexapyranose-based carbohydrates. J Comput Chem (submitted)

Lu X-J, Olson WK (2003) 3DNA: a software package for the analysis, rebuilding and visualization of three-dimensional nucleic acid structures. Nucleic Acids Res 31:5108–5121

MacCallum JL, Tieleman DP (2003) Calculation of the water-cyclohexane transfer free energies of neutral amino acid side-chain analogs using the OPLS all-atom force field. J Comput Chem 24:1930–1935

MacKerell Jr. AD, Wiórkiewicz-Kuczera J, Karplus M (1995) An all-atom empirical energy function for the simulation of nucleic-acids. J Am Chem Soc 117:11946–11975

MacKerell Jr AD, Bashford D, Bellot M, Dunbrack Jr. RL, Evanseck JD, Field MJ, Fischer S, Gao J, Guo H, Ha S, Joseph-McCarthy D, Kuchnir L, Kuczera K, Lau FTK, Mattos C, Michnick S, Ngo T, Nguyen DT, Prodhom B, Reiher III WE, Roux B, Schlenkrich M, Smith JC, Stote, R., Straub J, Watanabe M, Wiórkiewicz-Kuczera J, Yin D, Karplus M (1998) All-atom empirical potential for molecular modeling and dynamics studies of proteins. J Phys Chem B 102:3586–3616

Marelius J, Hansson T, Åqvist J (1998) Calculation of ligand binding free energies from molecular dynamics simulations. Int J Quantum Chem 69:77–88

Olson W, Bansal M, Burley SK, Dickerson RE, Gerstein M, Harvey SC, Heinemann U, Lu X-J, Neidle S, Shakked Z, Sklenar H, Suzuki M, Tung C-S, Westhof E, Wolberger C, Berman HM (2001) A standard reference frame for the description of nucleic acid base-pair geometry. J Mol Biol 313:229–237

Oostenbrink C, Gunsteren WF van (2004) Free energies of binding of polychlorinated biphenyls to the estrogen receptor from a single simulation. Proteins 54:237–246

Oostenbrink BC, Pitera JW, Van Lipzig MMH, Meerman JHN, Gunsteren WF van (2000) Simulations of the estrogen receptor ligand-binding domain: affinity of natural ligands and xenoestrogens. J Med Chem 43:4594–4605

Oostenbrink C, Villa A, Mark AE, Gunsteren WF van (2004) A biomolecular force field based on the free enthalpy of hydration and solvation: the GROMOS force-field parameter sets 53A5 and 53A6. J Comput Chem 25:1656–1676

Pearlman DA, Case DA, Caldwell JW, Ross WS, Cheatham III TE, DeBolt S, Ferguson D, Seibel G, Kollman PA (1995) AMBER, a package of computer-programs for applying molecular mechanics, normal-mode analysis, molecular-dynamics and free-energy calculations to simulate the structural and energetic properties of molecules. Comput Phys Comm 91:1–41

Peter C, Daura X, Gunsteren WF van (2000) Peptides of aminoxy acids: a molecular dynamics simulation of conformational equilibria under various conditions. J Am Chem Soc 122:7461–7466

Ryckaert J-P, Ciccotti G, Berendsen HJC (1977) Numerical integration of cartesian equations of motion of a system with constraints: molecular dynamics of n-alkanes. J Comput Phys 23:327–341

Schuler LD, Gunsteren WF van (2000) On the choice of dihedral angle potential energy functions for *n*-alkanes. Mol Simulat 25:301–319

Schuler LD, Daura X, Gunsteren WF van (2001) An improved GROMOS96 force field for aliphatic hydrocarbons in the condensed phase. J Comput Chem 22:1205–1218

Schwalbe H, Grimshaw SB, Spencer A, Buck M, Boyd J, Dobson CM, Redfield C, Smith LJ (2001) A refined solution structure of hen lysozyme determined using residual dipolar coupling data. Protein Sci 10:677–688

Scott WRP, Hünenberger PH, Tironi IG, Mark AE, Billeter SR, Fennen J, Torda AE, Huber P, Krüger P, Gunsteren WF van (1999) The GROMOS biomolecular simulation program package. J Phys Chem A 103:3596–3607

Shirts MR, Pitera JW, Swope WC, Pande VS (2003) Extremely precise free energy calculations of amino acid side chain analogs: Comparison of common molecular mechanics force fields for proteins. J Chem Phys 119:5740–5760

Shui X, McFail-Isom L, Hu GG, Dean Williams L (1998) The B-DNA dodecamer at high resolution reveals a spine of water on sodium. Biochemistry 37:8341–8355

Smith LJ, Sutcliffe MJ, Redfield C, Dobson CM (1991) Analysis of ϕ and χ_1 torsion angles for hen lysozyme in solution from ^{1}H NMR spin-spin coupling constants. Biochemistry 30:986–996

Smith LJ, Sutcliffe MJ, Redfield C, Dobson CM (1993) Structure of hen lysozyme in solution. J Mol Biol 229:930–944

Smith LJ, Mark AE, Dobson CM, Gunsteren WF van (1995) Comparison of MD simulations and NMR experiments for hen lysozyme: analysis of local fluctuations, cooperative motions and global changes. Biochemistry 34:10918–10931

Smith LJ, Dobson CM, Gunsteren WF van (1996) Side-chain conformational disorder in a molten globule: molecular dynamics simulations of the A-state of human alpha-lactalbumin. J Mol Biol 286:1567–1580

Smith LJ, Dobson CM, Gunsteren WF van (1999) Molecular dynamics simulations of human alpha-lactalbumin. Changes of the structural and dynamical properties of the protein at low pH. Proteins 36:77–86

Smith LJ, Berendsen HJC, Gunsteren WF van (2004) Computer simulation of urea-water mixtures: A test of force field parameters for use in biomolecular simulation. J Phys Chem A 108:1065–1071

Soares T, Daura X, Oostenbrink C, Smith LJ, van Gunsteren WF (2004) Validation of the GROMOS force-field parameter set 45A3 against nuclear magnetic resonance data of Hen Egg Lysozyme. J Biomol NMR 30:407–422

Soares TA, Hünenberger PH, Kastenholz MA, Kräutter V, Lenz T, Lins RD,Oostenbrink C, van Gunsteren WF (2005) An improved nucleic-acid parameter set for the GROMOS force field. J Comput Chem (in press)

Stocker U, Gunsteren WF van (2000) Molecular dynamics simulation of hen egg white lysozyme: a test of the GROMOS96 force field against nuclear magnetic resonance data. Proteins 40:145–153

Stocker U, Spiegel K, Gunsteren WF van (2000) On the similarity of properties in solution or in the crystalline state: a molecular dynamics study of hen lysozyme. J Biomol NMR 18:1–12

Talhout R, Villa A, Mark AE, Engberts JBFN (2003) Understanding binding affinity: a combined isothermal titration calorimetry/molecular dynamics study of the binding of a series of hydrophobically modified benzamidinium chloride inhibitors to trypsin. J Am Chem Soc 125:10570–10579

Tironi IG, Sperb R, Smith PE, Gunsteren WF van (1995) A generalized reaction field method for molecular-dynamics simulations. J Chem Phys 102:5451–5459

Tjandra N, Tate S, Ono A, Kainosho M, Bax A (2000) The NMR structure of a DNA dodecamer in an aqueous dilute crystalline phase. J Am Chem Soc 122:6190–6200

Tropp J (1980) Dipolar relaxation and nuclear Overhauser effects in nonrigid molecules: the effect of fluctuating internuclear distances. J Chem Phys 72:6035–6043

Vaney MC, Maignan S, RiesKautt M, Ducruix A (1996) High-resolution structure (1.33 angstrom) of a HEW lysozyme tetragonal crystal grown in the APCF apparatus. Data and structural comparison with a crystal grown under microgravity from SpaceHab-01 mission. Acta Cryst D52:505–517

Villa A, Mark AE (2002) Calculation of the free energy of solvation for neutral analogs of amino acid side chains. J Comput Chem 23:548–553

Walser R, Mark AE, Gunsteren WF van, Lauterbach M, Wipff G (2000) The effect of force-field parameters on properties of liquids: parametrization of a simple three-site model for methanol. J Chem Phys 112:10450–10459

Weiner PK, Kollman PA (1981) AMBER—assisted model-building with energy refinement—a general program for modeling molecules and their interactions. J Comput Chem 2:287–303

Wüthrich K, Billeter M, Braun W (1983) Pseudo-structures for the 20 common amino-acids for use in studies of protein conformations by measurements of intramolecular proton–proton distance constraints with nuclear magnetic resonance. J Mol Biol 169:949–961

Young MA, Jayaram B, Beveridge DL (1997) Intrusion of counterions into the spine of hydration in the minor groove of B-DNA: fractional occupancy of electronegative pockets. J Am Chem Soc 119:59–69